Draft version December 30, 2009
Preprint typeset using LaTeX style emulateapj v. 08/22/09

VIRIAL MASSES FROM THE HECTOSPEC CLUSTER SURVEY (HECS) AND THE SUNYAEV-ZELDOVICH EFFECT

Kenneth Rines[1,2], Margaret J. Geller[2], and Antonaldo Diaferio[3,4]

Draft version December 30, 2009

ABSTRACT

We present the first comparison of a large sample of virial masses of galaxy clusters with their Sunyaev-Zel'dovich (SZE) signals. We study 15 clusters from the Hectospec Cluster Survey (HeCS) with MMT/Hectospec spectroscopy and published SZE signals. We measure virial masses of these clusters from an average of 90 member redshifts inside the radius r_{100}. The virial masses of the clusters are strongly correlated with their SZE signals (at the 99% confidence level using a Spearman rank-sum test). This correlation suggests that Y_{SZ} can be used as a measure of virial mass. Simulations predict a powerlaw scaling of $Y_{SZ} \propto M_{200}^{\alpha}$ with $\alpha \approx 1.6$. Observationally, we find $\alpha = 1.11 \pm 0.16$, significantly shallower than the theoretical prediction. More detailed studies of scaling relations may be needed to understand the relation between cluster mass and SZ signal.

Subject headings: galaxies: clusters: individual — galaxies: kinematics and dynamics — cosmology: observations

1. INTRODUCTION

Clusters of galaxies are the most massive virialized systems in the universe. The normalization and evolution of the cluster mass function is therefore a sensitive probe of the growth of structure and thus cosmology (e.g., Rines et al. 2007, 2008; Vikhlinin et al. 2009; Henry et al. 2009; Mantz et al. 2008; Rozo et al. 2008, and references therein). Many methods exist to estimate cluster masses, including dynamical masses from either galaxies (Zwicky 1937) or intracluster gas (e.g., Fabricant et al. 1980), gravitational lensing (e.g., Smith et al. 2005; Richard et al. 2010), and the Sunyaev-Zel'dovich effect (SZE Sunyaev & Zeldovich 1972). In practice, these estimates are often made using simple observables, such as velocity dispersion for galaxy dynamics or X-ray temperature for the intracluster gas. If one of these observable properties of clusters has a well-defined relation to the cluster mass, a large survey can yield tight constraints on cosmological parameters (e.g., Majumdar & Mohr 2004). There is thus much interest in identifying cluster observables that exhibit tight scaling relations with mass (Kravtsov et al. 2006; Rozo et al. 2008). Numerical simulations indicate that X-ray gas observables (Nagai et al. 2007) and SZE signals (Motl et al. 2005) are both candidates for tight scaling relations. Both methods are beginning to gain observational support (e.g., Henry et al. 2009; Lopes et al. 2009; Mantz et al. 2009; Locutus Huang et al. 2009).

Here, we make the first comparison between virial masses of galaxy clusters and their SZE signals. We use SZ measurements from the literature and newly-measured virial masses of 15 clusters from extensive MMT/Hectospec spectroscopy. This comparison tests the robustness of the SZE as a proxy for cluster mass and the physical relationship between the SZE signal and cluster mass.

We assume a cosmology of $\Omega_m = 0.3$, $\Omega_\Lambda = 0.7$, and $H_0 = 70$ km s^{-1} Mpc^{-1} for all calculations.

2. OBSERVATIONS

2.1. *Optical Photometry and Spectroscopy*

We are completing the Hectospec Cluster Survey (HeCS), a study of an X-ray flux-limited sample of 53 galaxy clusters at moderate redshift with extensive spectroscopy from MMT/Hectospec. We selected HeCS clusters from their X-ray emission as measured by the ROSAT All-Sky Survey (RASS, Voges et al. 1999). We use photometry from the Sixth Data Release of SDSS (Adelman-McCarthy et al. 2008) to select Hectospec targets. The HeCS targets are all brighter than $r = 20.8$ (SDSS catalogs are 95% complete for point sources to $r \approx 22.2$). Out of the HeCS sample, 15 clusters have published SZ measurements.

2.1.1. *Spectroscopy: MMT/Hectospec and SDSS*

HeCS is a spectroscopic survey of clusters in the redshift range $0.10 \leq z \leq 0.30$. We measure spectra with the Hectospec instrument (Fabricant et al. 2005) on the MMT 6.5m telescope. Hectospec provides simultaneous spectroscopy of up to 300 objects across a diameter of 1°. This telescope and instrument combination is ideal for studying the virial regions and outskirts of clusters at these redshifts. We use the red sequence to preselect likely cluster members as primary targets, and we fill fibers with bluer targets (Rines et al. in prep. describes the details of target selection). We eliminate all targets with existing SDSS spectroscopy from our target lists but include these in our final redshift catalogs.

Of the 15 clusters studied here, one was observed with a single Hectospec pointing and the remaining 14 were observed with two pointings. Using multiple pointings and incorporating SDSS redshifts of brighter objects mitigate fiber collision issues. Because the galaxy targets are relatively bright ($r \leq 20.8$), the spectra were obtained with

Electronic address: kenneth.rines@wwu.edu
[1] Department of Physics & Astronomy, Western Washington University, Bellingham, WA 98225; kenneth.rines@wwu.edu
[2] Smithsonian Astrophysical Observatory, 60 Garden St, Cambridge, MA 02138
[3] Università degli Studi di Torino, Dipartimento di Fisica Generale "Amedeo Avogadro", Torino, Italy
[4] Istituto Nazionale di Fisica Nucleare (INFN), Sezione di Torino, Torino, Italy

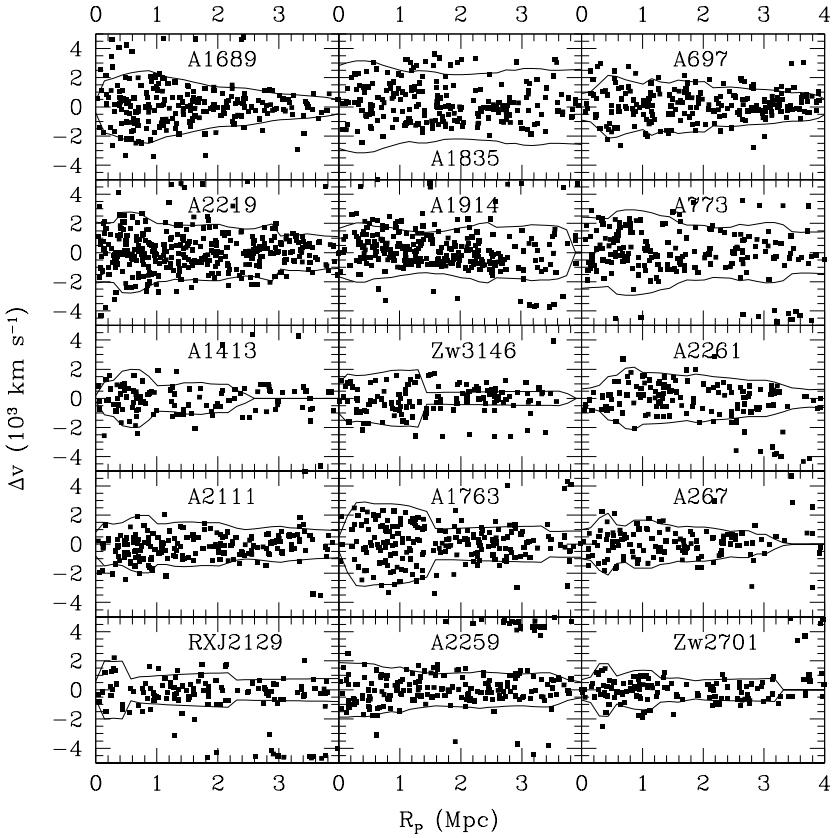

FIG. 1.— Redshift versus projected clustrocentric radius for the 15 HeCS clusters studied here. Clusters are ordered by decreasing $Y_{SZ}D_A^2(r_{2500})$ left-to-right and top-to-bottom. The solid lines show the locations of the caustics, which we use to identify cluster members. The Hectospec data extend out to ∼8 Mpc; the figure shows only the inner 4 Mpc to focus on the virial regions.

relatively short exposure times of 3x600s to 4x900s under a variety of observing consitions.

Figure 1 shows the redshifts of galaxies versus their projected clustrocentric radii. The infall patterns are clearly present in all clusters. We use the caustic technique (Diaferio 1999) to determine cluster membership. Briefly, the caustic technique uses a redshift-radius diagram to isolate cluster members in phase space by using an adaptive kernel estimator to smooth out the galaxies in phase space, and then determining the edges of this distribution (see Diaferio 2009, for a recent review). This technique has been successfully applied to optical studies of X-ray clusters, and yields cluster mass estimates in agreement with estimates from X-ray observations and gravitational lensing (e.g., Rines et al. 2003; Diaferio et al. 2005; Rines & Diaferio 2006; Rines et al. 2007, and references therein).

We apply the prescription of Danese et al. (1980) to determine the mean redshift $cz_\odot$ and projected velocity dispersion σ_p of each cluster from all galaxies within the caustics. We calculate σ_p using only the cluster members projected within r_{100} estimated from the caustic mass profile.

2.2. *SZE Measurements*

The SZE detections are primarily from Bonamente et al. (2008, hereafter B08), supplemented by three measurements from Marrone et al. (2009, hereafter M09). Most of the SZ data were obtained with the OVRO/BIMA arrays; the additional clusters from M09 were observed with the Sunyaev-Zel'dovich Array (SZA; e.g., Muchovej et al. 2007).

Numerical simulations indicate that the integrated Compton y-parameter Y_{SZ} has smaller scatter than the peak y-decrement y_{peak} (Motl et al. 2005), so B08 and M09 report only Y_{SZ}. Although y_{peak} should be nearly independent of redshift, Y_{SZ} depends on the angular size of the cluster. The quantity $Y_{SZ}D_A^2$ removes this dependence. Thus, we compare our dynamical mass estimates to this quantity rather than y_{peak} or Y_{SZ}. Table 1 summarizes the SZ data and optical spectroscopy.

It is also critical to determine the radius within which Y_{SZ} is determined. B08 use r_{2500}, the radius that encloses an average density of 2500 times the critical density at the cluster's redshift; r_{2500} has physical values of 300-700 kpc for the massive clusters studied by B08 (470-670 kpc for the subsample studied here). M09 use a physical radius of 350 kpc because this radius best matches their lensing data.

To use both sets of data, we must estimate the conversion between $Y_{SZ}(r_{2500})$ measured within r_{2500} and $Y_{SZ}(r = 350$ kpc) measured within the smaller radius $r =$350 kpc. There are 8 clusters analyzed in both B08 and M09 (5 of which are in HeCS). We perform a least-squares fit to $Y_{SZ}(r_{2500}) - Y_{SZ}(r = 350\text{kpc})$ to determine an approximate aperture correction for the M09 clusters. We list both quantities in Table 1.

TABLE 1
HeCS Dynamical Masses and SZE Signals

Cluster	z	σ_p	$M_{100,v}$	$M_{100,c}$	$Y_{SZ}D_A^2$ (350 kpc)	$Y_{SZ}D_A^2$ (r_{2500})	SZE
		km s^{-1}	$10^{14}M_\odot$	$10^{14}M_\odot$	10^{-5}Mpc^{-2}	10^{-4}Mpc^2	Ref.
A267	0.2288	743^{+81}_{-61}	4.80±0.58	2.98±0.10	3.08±0.34	0.42±0.06	1
A697	0.2812	784^{+77}_{-59}	4.28±0.48	4.17±2.46	–	1.29±0.15	1
A773	0.2174	1066^{+77}_{-63}	12.9±1.2	11.4±0.5	5.40±0.57	0.90±0.10	1
Zw2701	0.2160	564^{+63}_{-47}	2.43±0.30	1.88±0.21	1.46±0.016	0.17±0.02[a]	2
Zw3146	0.2895	752^{+92}_{-67}	4.81±0.62	3.47±0.64	–	0.71±0.09	1
A1413	0.1419	674^{+81}_{-60}	4.62±0.59	2.44±0.11	3.47±0.24	0.81±0.12	1
A1689	0.1844	886^{+63}_{-52}	10.7±0.9	6.61±3.96	7.51±0.60	1.50±0.14	1
A1763	0.2315	1042^{+79}_{-64}	11.8±1.1	8.81±1.08	3.10±0.32	0.46±0.05[a]	2
A1835	0.2507	1046^{+66}_{-55}	13.7±1.1	14.4±0.2	6.82±0.48	1.37±0.11	1
A1914	0.1659	698^{+46}_{-38}	4.69±0.40	4.35±0.14	–	1.08±0.09	1
A2111	0.2290	661^{+57}_{-45}	2.81±0.29	3.34±0.86	–	0.55±0.12	1
A2219	0.2256	915^{+53}_{-45}	8.96±0.69	8.38±0.33	6.27±0.26	1.19±0.05[a]	2
A2259	0.1606	735^{+67}_{-53}	3.91±0.42	3.43±1.18	–	0.27±0.10	1
A2261	0.2249	725^{+75}_{-57}	4.99±0.58	3.57±1.45	–	0.71±0.09	1
RXJ2129	0.2338	684^{+88}_{-64}	3.02±0.40	2.06±0.09	–	0.40±0.07	1

Note. — Redshift z and velocity dispersion σ_p are computed for galaxies defined as members using the caustics. Masses $M_{100,v}$ and $M_{100,c}$ are evaluated using the virial mass profile and caustic mass profile respectively.

Note. — REFERENCES: SZE data are from (1) Bonamente et al. 2008 and (2) Marrone et al. 2009.

[a]Extrapolated to r_{2500} using the best-fit relation between $Y_{SZ}D_A^2$(350kpc) and $Y_{SZ}D_A^2(r_{2500})$ for eight clusters in common between B08 and M09.

3. RESULTS

We examine two issues: (1) the strength of the correlation between SZE signal and the dynamical mass and (2) the slope of the relationship between them. Figure 2 shows the $Y_{SZ}-\sigma_p$ relation. Here, we compute σ_p for all galaxies inside both the caustics and the radius $r_{100,c}$ defined by the caustic mass profile [r_δ is the radius within which the enclosed density is δ times the critical density $\rho_c(z)$].

Because we make the first comparison of dynamical properties and SZE signals for a large cluster sample, we first confirm that these two variables are well correlated. A nonparametric Spearman rank-sum test (one-tailed) rejects the hypothesis of uncorrelated data at the 98.4% confidence level. The strong correlation in the data suggests that both σ_p and $Y_{SZ}D_A^2$ increase with increasing cluster mass.

Hydrodynamic numerical simulations indicate that Y_{SZ} (integrated to r_{500}) scales with cluster mass as $Y_{SZ} \propto M_{500}^{\alpha}$, where α=1.60 with radiative cooling and star formation, and 1.61 for simulations with radiative cooling, star formation, and AGN feedback (α=1.70 for non-radiative simulations, Motl et al. 2005). Combining this result with the virial scaling relation of dark matter particles, $\sigma_p \propto M_{200}^{0.336\pm0.003}$ (Evrard et al. 2008), the expected scaling is $Y_{SZ} \propto \sigma^{4.76}$ (we assume that $M_{100} \propto M_{500}$). The right panels of Figure 2 shows this predicted slope (dashed lines).

The bisector of the least-squares fits to the data has a slope of 2.94 ± 0.74, significantly shallower than the predicted slope of 4.8.

We recompute the velocity dispersions $\sigma_{p,A}$ for all galaxies within one Abell radius (2.14 Mpc) and inside the caustics. Surprisingly, the correlation is slightly stronger (99.4% confidence level). This result supports the idea that velocity dispersions computed within a fixed physical radius retain strong correlations with other cluster observables, even though we measure the velocity dispersion inside different fractions of the virial radius for clusters of different masses. Because cluster velocity dispersions decline with radius (e.g. Rines et al. 2003; Rines & Diaferio 2006), $\sigma_{p,A}$ may be smaller than $\sigma_{p,100}$ (measured within $r_{100,c}$) for low-mass clusters, perhaps exaggerating the difference in measured velocity dispersions relative to the differences in virial mass (i.e., $\sigma_{p,A}$ of a low-mass cluster may be measured within $2r_{100}$ while $\sigma_{p,A}$ of a high-mass cluster may be measured within r_{100}; the ratio $\sigma_{p,A}$ of these clusters would be exaggerated relative to the ratio $\sigma_{p,100}$). Future cluster surveys with enough redshifts to estimate velocity dispersions but too few to perform a caustic analysis should still be sufficient for analyzing scaling relations.

Because of random errors in the mass estimation, the virial mass and the caustic mass within a given radius do not necessarily coincide. Therefore, the radius r_{100} depends on the mass estimator used. Figure 2 shows the scaling relations for two estimated masses $M_{100,c}$ and $M_{100,v}$; $M_{100,c}$ is the mass estimated within $r_{100,c}$ (where both quantities are defined from the caustic mass profile), and $M_{100,v}$ is the mass estimated within $r_{100,v}$ (both quantities are estimated with the virial theorem, e.g., Rines & Diaferio 2006). Similar to σ_p, there is a clear correlation between $M_{100,v}$ and $Y_{SZ}D_A^2$ (99.0% confidence with a Spearman test). The strong correlation of dynamical mass with SZE also holds for $M_{100,c}$ estimated directly from the caustic technique (99.8% confidence).

The bisector of the least-squares fits has a slope of 1.11 ± 0.16, again significantly shallower than the pre-

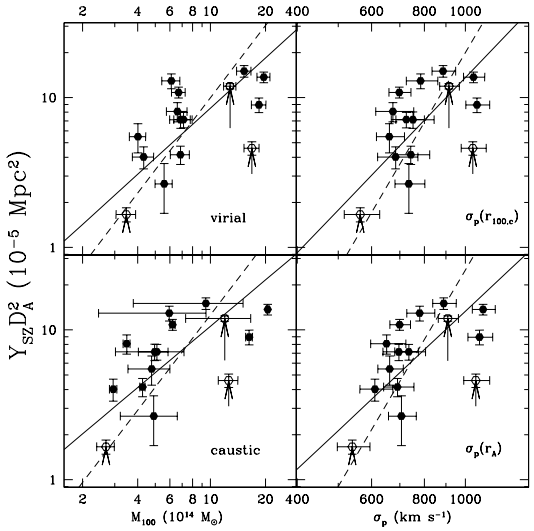

FIG. 2.— Integrated S-Z Compton parameter $Y_{SZ}D_A^2$ versus dynamical properties for 15 clusters from HeCS. *Left panels:* SZE data versus virial mass M_{100} estimated from the virial mass profile (top) and the caustic mass profile (bottom). Solid and open points indicate SZ measurements from B08 and M09 respectively. The dashed line shows the slope of the scaling predicted from numerical simulations: $Y_{SZ} \propto M^{1.6}$ (Motl et al. 2005), while the solid line shows the ordinary least-squares bisector. Arrows show the aperture corrections to the SZE measurements (see text). *Right panels:* SZE data versus projected velocity dispersions measured for galaxies inside the caustics and (top) inside $r_{100,c}$ estimated from the caustic mass profile and (bottom) inside the Abell radius 2.14 Mpc. The dashed line shows the scaling predicted from simulations: $Y_{SZ} \propto M^{1.6}$ (Motl et al. 2005) and $\sigma \propto M^{0.33}$ (Evrard et al. 2008). The solid line shows the ordinary least-squares bisector. Data points and arrows are defined as in the left panels.

dicted slope of 1.6. The origin of this discrepancy is unclear. The sample we study here is small and may have selection biases. Larger samples should determine whether unknown observational biases or issues in the physical understanding of the relation account for this discrepancy.

4. DISCUSSION

The strong correlation between masses from galaxy dynamics and SZE signals indicates that the SZE is a reasonable proxy for cluster mass. B08 compare SZE signals to X-ray observables, in particular the temperature T_X of the intracluster medium and $Y_X = M_{gas}T_X$, where M_{gas} is the mass of the ICM. Both of these quantities are measured within r_{500}, a significantly smaller radius than r_{100} where we measure virial mass. M09 compare SZE signals to masses estimated from gravitational lensing measurements. The lensing masses are measured within a radius of 350 kpc. For the clusters studied here, this radius is smaller than r_{2500} and much smaller than r_{100}. Numerical simulations indicate that the scatter in masses measured within an overdensity δ decreases as δ decreases (White 2002), largely because variations in cluster cores are averaged out at larger radii. Thus, the dynamical measurement reaching to larger radius may provide a more robust indication of the relationship between the SZE measurements and cluster mass.

The $Y_{SZ}D_A^2 - M_{lens}$ data presented in M09 show a weaker correlation than our optical dynamical properties. A Spearman test rejects the hypothesis of uncorrelated data for the M09 data at only the 94.8% confidence level, compared to the 98.4-99.8% confidence levels for our optical dynamical properties. One possiblility is that M_{lens} is more strongly affected by substructure in cluster cores and by line-of-sight structures than are the virial masses and velocity dispersions we derive.

5. CONCLUSIONS

Our first direct comparison of virial masses, velocity dispersions, and SZ measurements for a sizable cluster sample demonstrates a strong correlation between these observables (98.4-99.8% confidence). The SZE signal increases with cluster mass. However, the slopes of both the $Y_{SZ} - \sigma$ relation ($Y_{SZ} \propto \sigma_p^{2.94\pm0.74}$) and the $Y_{SZ} - M_{100}$ relation ($Y_{SZ} \propto M_{100}^{1.11\pm0.16}$) are significantly shallower than the slopes predicted by numerical simulations (4.76 and 1.60 respectively).

Curiously, Y_{SZ} is more strongly correlated with both σ and M_{100} than with M_{lens} (M09). Comparison of lensing masses and cluster velocity dispersions (and virial masses) for larger, complete, objectively selected samples of clusters may resolve these differences.

The full HeCS sample of 53 clusters will provide a large sample of clusters with robustly measured velocity dispersions and virial masses as a parial foundation for these comparisons.

AD gratefully acknowledges partial support from INFN grant PD51.

Facilities: MMT (Hectospec)

REFERENCES

Adelman-McCarthy, J. K. et al. 2008, ApJS, 175, 297
Bonamente, M., Joy, M., LaRoque, S. J., Carlstrom, J. E., Nagai, D., & Marrone, D. P. 2008, ApJ, 675, 106
Danese, L., de Zotti, G., & di Tullio, G. 1980, A&A, 82, 322
Diaferio, A. 1999, MNRAS, 309, 610
—. 2009, ArXiv e-prints
Diaferio, A., Geller, M. J., & Rines, K. J. 2005, ApJ, 628, L97
Evrard, A. E. et al. 2008, ApJ, 672, 122
Fabricant, D., Lecar, M., & Gorenstein, P. 1980, ApJ, 241, 552
Fabricant, D. et al. 2005, PASP, 117, 1411
Henry, J. P., Evrard, A. E., Hoekstra, H., Babul, A., & Mahdavi, A. 2009, ApJ, 691, 1307
Kravtsov, A. V., Vikhlinin, A., & Nagai, D. 2006, ApJ, 650, 128
Locutus Huang, C. et al. 2009, ArXiv e-prints
Lopes, P. A. A., de Carvalho, R. R., Kohl-Moreira, J. L., & Jones, C. 2009, ArXiv e-prints
Majumdar, S. & Mohr, J. J. 2004, ApJ, 613, 41
Mantz, A., Allen, S. W., Ebeling, H., & Rapetti, D. 2008, MNRAS, 387, 1179
Mantz, A., Allen, S. W., Ebeling, H., Rapetti, D., & Drlica-Wagner, A. 2009, ArXiv e-prints
Marrone, D. P. et al. 2009, ApJ, 701, L114
Motl, P. M., Hallman, E. J., Burns, J. O., & Norman, M. L. 2005, ApJ, 623, L63
Muchovej, S. et al. 2007, ApJ, 663, 708
Nagai, D., Vikhlinin, A., & Kravtsov, A. V. 2007, ApJ, 655, 98
Richard, J. et al. 2010, ArXiv e-prints
Rines, K. & Diaferio, A. 2006, AJ, 132, 1275
Rines, K., Diaferio, A., & Natarajan, P. 2007, ApJ, 657, 183
—. 2008, ApJ, 679, L1
Rines, K., Geller, M. J., Kurtz, M. J., & Diaferio, A. 2003, AJ, 126, 2152

Rozo, E. et al. 2008, astro-ph/0703571
Smith, G. P., Kneib, J., Smail, I., Mazzotta, P., Ebeling, H., & Czoske, O. 2005, MNRAS, 359, 417
Sunyaev, R. A. & Zeldovich, Y. B. 1972, Comments on Astrophysics and Space Physics, 4, 173
Vikhlinin, A. et al. 2009, ApJ, 692, 1060
Voges, W. et al. 1999, A&A, 349, 389
White, M. 2002, ApJS, 143, 241
Zwicky, F. 1937, ApJ, 86, 217